JOURNAL OF GEOPHYSICAL RESEARCH, VOL. 105, NO. C9, PAGES 22,035–22,047, SEPTEMBER 15, 2000

Spectral analysis of turbulent flow and suspended sediment transport over fixed dunes

Jeremy G. Venditti

Department of Geography, University of British Columbia, Vancouver, British Columbia, Canada

Sean J. Bennett

National Sedimentation Laboratory, Agricultural Research Service, U.S. Department of Agriculture, Oxford, Mississippi

Abstract. Laboratory measurements of turbulent fluctuations in velocity and suspended sediment concentration were obtained synchronously over fixed two-dimensional dunes in a sediment-starved flow. Contour maps of turbulent flow parameters demonstrate that the flow separation cell and a perturbed shear layer are the main sources of turbulence production and that the distribution of suspended sediment is controlled by spatially dependent macroturbulent flow structures. Spectral analysis reveals that peak spectral energies generally occur at 1-2 Hz for the streamwise velocity component and 2-4 Hz for the cross-stream and vertical velocity components. Spectra show larger and better defined energy peaks near the shear layer. Peak spectral energies for suspended sediment concentration occur near 1 Hz throughout the flow. Squared coherency values for co-spectral analysis of velocity and sediment concentration are insignificant. Integral timescales for velocity range from 0.20 s for the streamwise component to 0.06 s for the cross-stream and vertical components. Integral length scales for velocity range from 0.065 to 0.135 m for the streamwise component, which is comparable to flow depth, and from 0.020 to 0.030 m for the cross-stream and vertical components, which is comparable to dune height. For suspended sediment concentration, integral timescales and length scales are similar to the streamwise velocity component.

1. Introduction

Dunes are the most common bed configuration in sand-bedded streams. The dimensions and migration rates of dunes control bed load transport rates and their presence significantly impacts total flow resistance. Dunes also interact with the turbulent flow field, and several studies have described the macroturbulent characteristics of spatially varied flow over these bed forms [*Nelson et al.*, 1993; *McLean et al.*, 1994; *Bennett and Best*, 1995; *McLean et al.*, 1996]. Examining the complex interaction between turbulent flow, bed topography, and sediment flux will lead to an improved understanding of bed form stability, transition, and more generally, flow and sediment transport processes in river channels [see *Best*, 1996, *Ashworth et al.*, 1996; *Parker*, 1996].

Macroturbulent flow over dunes strongly affects suspended sediment transport processes. Phenomena such as "kolks" and "boils," which are circular upwellings of both fluid and sediment, appear to be related to macroturbulent events and to originate along the shear layer downstream of dune crests and at the point of flow reattachment [*Matthes*, 1947; *Korchokha*, 1968; *Coleman*, 1969; *Jackson*, 1976; *Müller and Gyr*, 1982, 1986; *Iseya*, 1984; *Iseya and Ikeda*, 1986; *Babakaiff and Hickin*, 1996]. These periodic motions can cause orders of magnitude variations in suspended sediment transport rates at a point and are thought to be responsible for much of the vertical mixing in rivers [*Lapointe*, 1992; *Kostaschuk and Church*, 1993]. Studies using optical and acoustic sensors in estuaries and coastal waters also have highlighted the importance of macroturbulent events in transporting sediment in near-bed regions [*Hay and Sheng*, 1992; *Lapointe*, 1992, 1996; *Thorne et al.*, 1993, 1996]. These observations have demonstrated that pure gradient diffusion is an inappropriate model for predicting the distribution of suspended sediment in these turbulent shear flows and that periodic convection of sediment within or associated with macroturbulent events must also be considered [see *Nielsen*, 1992, 1994].

In spite of considerable success in quantifying macroturbulent events and their effect on suspended sediment transport the dynamics of this interaction remains poorly understood. Moreover, the frequency and scaling of large-scale sediment-laden turbulent motions have not been resolved. Acquisition of coincident time series of turbulent fluctuations in velocity and suspended sediment concentration have afforded opportunities to use spectral and cospectral analyses to examine the link between turbulence and suspended sediment flux.

Spectral analysis has been applied to examine the characteristics of suspended sediment transport under waves in near-shore environments. *Osborne and Greenwood* [1991a, 1991b, 1993] have used spectral and cospectral analyses to determine the link between sediment transport and near-bed wave velocity. Their results show that the vertical convection of sediment can be related to ejections of fluid in the wave boundary layer over bed forms. *Hay and Bowen* [1994] have also applied time series analysis to examine suspended sediment transport scaling in the surf zone. They have shown a relation between sediment flux and large-scale eddies generated under longshore currents over dunes whose crests were oriented in a shore normal direction.

Paper number 2000JC900094.
0148-0227/00/2000JC900094$09.00

Table 1. Summary of Hydraulic and Bed Conditions for the Experiment

Parameter	Value
Dune height H, m	0.040
Dune length λ, m	0.600
Dune height-to-depth ratio, H/d	0.229
Dune height-to-length ratio, H/λ	0.067
Slip face angle, deg	30
Width, m	1.000
Mean depth d, m	0.175
Maximum depth, m	0.194
Mean flow velocity $\bar{v}$, m s^{-1}	0.458
Maximum flow velocity, m s^{-1}	0.625
Discharge, m s^{-3}	0.079
Water surface slope S	0.00181
Froude number Fr	0.350
Reynolds number Re	8.0×10^4
Bed shear stress τ_0, Pa	2.31
Shear Velocity u_*, m s^{-1}	0.048
Darcy-Weisbach friction factor ff	0.088
From Reynolds Stress Profile:	
τ_R, Pa	1.69
u_{*R}, m s^{-1}	0.041
ff_R	0.064
Mean suspended sediment concentration, mg L^{-1}	141.9
Mean suspended sediment transport rate, kg m^{-1} s^{-1}	0.065

Laboratory experiments by *Ikeda and Asaeda* [1983] correlated sediment concentration energy spectra peaks with turbulent bursting periodicity scaled by outer boundary variables in the lee of ripples. Similar attempts to link turbulent motions to suspended sediment transport using spectral and cospectral analyses have been made in rivers with modest success [e.g., *Lapointe*, 1992, 1996].

The present paper examines turbulent flow over dune bed forms in a laboratory channel and the link between macroturbulence and suspended sediment flux. The objectives the study were (1) to describe the characteristics of turbulent flow and suspended sediment transport over dunes, (2) to determine the frequency and size of coherent flow structures (macroturbulence) using spectral and cospectral techniques, and (3) to define the link between turbulent fluctuations in velocity and suspended sediment flux.

2. Experimental Equipment and Procedure

The experiment was conducted at the National Sedimentation Laboratory, U.S. Department of Agriculture, Oxford, Mississippi, using a tilting recirculating flume 15.2 m long, 1 m wide, and 0.25 m deep. Twenty-four two-dimensional steel dunes 0.6 m long and 0.04 m high, with a slip face angle of 30°, were fixed to the floor of the flume, covering almost 95% of the flume length.

A necessary prerequisite for examining turbulent flow over fixed bed forms is employing a flow stage similar to that experienced by equilibrium mobile dunes of identical size [see *Bennett and Best*, 1995]. On the basis of previous studies [*Guy et al.*, 1966; *Flemming*, 1988; *van Rijn*, 1994] a Froude number ($Fr = \bar{U}/(gd)^{0.5}$, where $\bar{U}$ is mean streamwise flow velocity, g is gravitational acceleration, and d is mean flow depth) of 0.35 was selected as an appropriate flow criterion for these bed forms. Mean flow velocity, mean flow depth, and discharge were set to 0.458 m s^{-1}, 0.175 m, and 0.079 m^3 s^{-1}, respectively, so that the dune height to flow depth ratio ($H/d = 0.229$) and dune height to length ratio ($H/\lambda = 0.067$) agree well with those observed in previous studies (see review given by *Bennett and Best* [1995]). Flow discharge was monitored using a differential pressure transducer connected to ports about an in-line orifice plate. Quasi-equilibrium flow was achieved by adjusting the slope to attain the same flow depth to within ±2 mm over five successive bed form crests. Mean water surface slope S over a length of 5.4 m of the flume was 0.00181, mean boundary shear stress ($\tau_0 = \rho g R S$, where ρ is fluid density and R is the hydraulic radius) was 2.31 Pa, shear velocity ($u_* = (\tau_0/\rho)^{0.5}$) was 0.041 m s^{-1}, friction factor ($ff = 8\tau_0/\rho\bar{U}^2$) was 0.087, and flow Reynolds number ($Re = \bar{U}d/\nu$, where ν is the kinematic viscosity of the fluid) was 8.0×10^4. Table 1 summarizes the hydraulic and bed conditions for the experiment.

Approximately 20 kg of well-sorted sand with a median diameter of 0.1 mm and fall velocity ω_s of 0.008 m s^{-1} was added to the flow. While both bed load and suspended load transport were observed, the flow was starved of sediment. The addition of sediment to the flow has the potential to alter the characteristics of the turbulence (see review given by *Best et al.* [1997]). Although no measurements were made in equivalent clear water flows, turbulence modulation is expected to be minimal on the basis of the grain size and the concentration of sediment used. Some sediment was deposited on the dune slip faces during the experiment, and this was periodically removed. Equilibrium

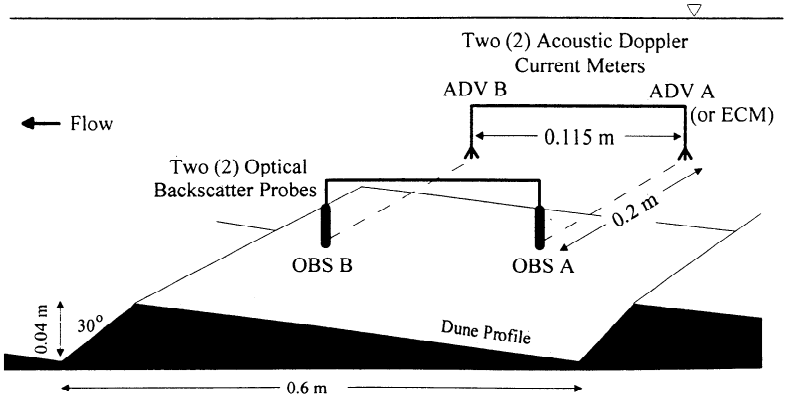

Figure 1. Schematic of the dune topography and instrument positions.

vertical profiles of suspended sediment concentration for a flat bed flow is expected at a distance of $\bar{u}d/\omega_s \geq 10\,\mathrm{m}$ from the flume headbox [*Willis*, 1969]. The mean suspended sediment concentration through the test section was 141.9 mg L^{-1} (0.065 kg m^{-1} s^{-1}; see below).

All flow sensors and turbidity probes were mounted on a movable carriage on rails mounted on the flume sidewalls. Velocity measurements were obtained using two acoustic Doppler velocimeters (ADVs) and one electromagnetic current meter (ECM). The ADVs measure three-component flow velocities at 25 Hz, have a reported accuracy of ±0.1 mm s^{-1}, and have focal lengths of 0.053 and 0.058 m. These probes were mounted in a plane parallel to the flow direction and spaced 0.115 m apart (Figure 1). ADV signals are affected by Doppler noise, or white noise, associated with the measurement process [*Lohrmann et al.*, 1994]. The presence of this noise at high frequencies may create an aliasing effect in frequencies greater than the Nyquist frequency (herein $f_n = 12.5\,\mathrm{Hz}$). To remove possible aliasing effects, a Gaussian low-pass filter with a half-power frequency of 12.5 Hz was applied to the velocity time series, removing all variance at frequencies above f_n [*Biron et al.*, 1995; *Lane et al.*, 1998]. To correct for misalignment of the velocity probe, it is also common to rotate velocity signals to maximize the mean streamwise velocity. However, the sensor position was carefully aligned with reference to the flume centerline so no rotations were applied. The ECM measures two-component flow velocities at 5 Hz about its 12.5 mm diameter probe head and has a reported accuracy of ±9 mm s^{-1}. In the present application, only the streamwise component was measured in the near-surface flow region.

Two optical backscatter probes (OBS) were mounted perpendicular to the flow direction and oriented toward the ADV sampling volumes at a distance of 0.2 m (Figures 1 and 2). OBS probes measure water turbidity, hence sediment concentration, and a sampling rate of 10 Hz was used. These probes operate by transmitting an infrared signal and measuring the strength of backscatterance by particles in the flow; hence the probes need to be at least 0.2 m from any solid object. For sediment of uniform size their response is linear over a wide range of concentrations [e.g., *Lapointe*, 1992]. OBS probes are unaffected by visible portions of the electromagnetic spectrum but are susceptible to

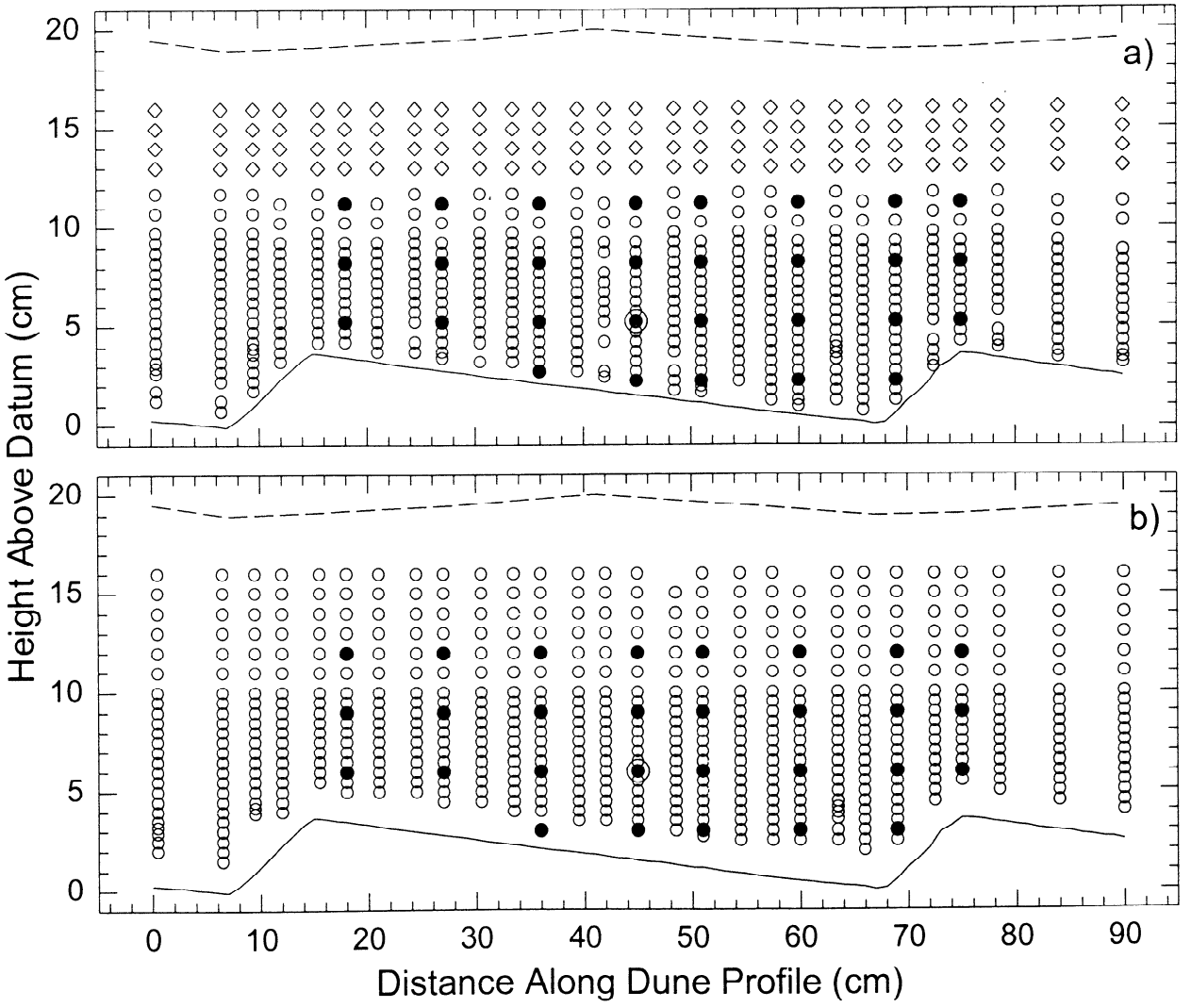

Figure 2. Locations of (a) ADV (circles) and ECM (diamonds) velocity and (b) OBS turbidity measurements. The solid circles indicate points where spectral analysis was performed, and the circled symbols indicate where cospectral analysis was performed. The solid line is the bed profile, and the dashed line is the water surface profile.

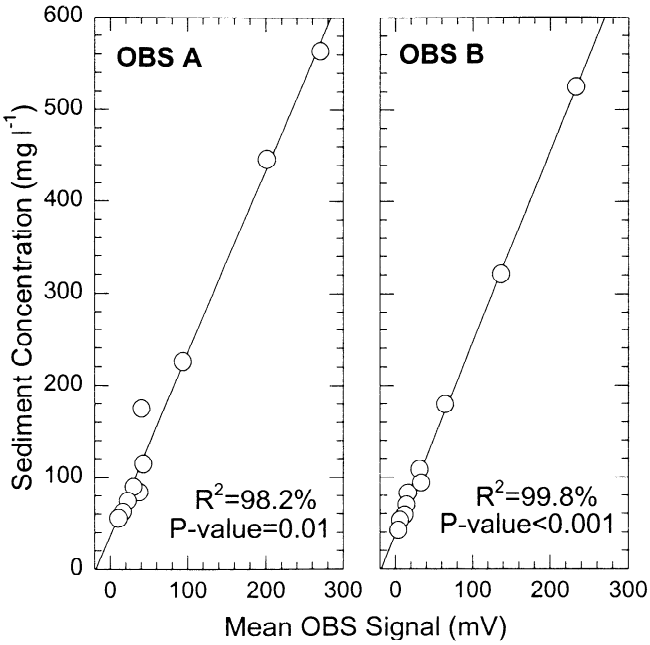

Figure 3. Calibration curves relating the mean analog OBS signal to time-averaged suspended sand concentration.

the infrared band. Sediment-laden laboratory flows have low infrared transmission and are not susceptible to contamination by external sources [*van Rijn*, 1994].

Instrument gain and zero values for each OBS probe were adjusted for the present conditions. Calibration was accomplished by obtaining vertical profiles of turbidity in conjunction with direct sampling of the suspended sediment concentrations at 14-18 positions. A mixture of water and sediment was siphoned at each point using a 4 mm diameter copper tube that was placed into the flow and oriented parallel to the mean flow direction. Approximately 0.5 L of fluid and sediment were extracted over a period of ~60 s, and each sample was decanted, oven dried, and weighed to determine total sediment mass. Regression analysis derived the relationship between turbidity and sediment concentration for each probe in mg L^{-1} (Figure 3). The zero value for the OBS probes was user-defined and zero voltage did not correspond to zero sediment concentration. Because the experiment was conducted over several days, water quality, hence turbidity, varied, causing some drift in the concentration data. Therefore each concentration profile was normalized by the profile mean and then multiplied by the spatially averaged concentration. This water quality correction adjusted the time series so that accurate values of mean sediment concentration could be obtained. The characteristics of signal variance remained unaffected.

A 0.90 m test section was established over the twentieth dune, 12 m downstream of the flume entrance. A total of 28 profiles of velocity and sediment concentration were taken along the centerline of the flume and spaced 0.025-0.035 m apart, each profile consisting of 15-20 vertical measurement locations (Figure 2 shows ADV and OBS positions). Velocity and concentration were sampled for 120 s at each point. The lowest point in each velocity profile was 0.005 m above the bed. Because of their minimum working depth, these ADV probes were restricted to the lower 0.12 m ($z/d \leq 0.69$, where z is height above the bed) of the flow field.

Each ADV had a dedicated computer, and the ECM and all OBS probes were linked to a data acquisition board in another computer. The OBS signals were time-synchronized with the two ADVs using a configuration where one ADV sent a 5 V signal to initiate data collection at all probes. Time drift in the computer clocks was considered negligible because each concomitant data string was only 120 s long.

3. Mean Turbulent Flow and Suspended Sediment Concentration

3.1. Mean Flow Field

The mean and turbulent flow structures over fixed dunes have been described previously [*Nelson et al.*, 1993; *McLean et al.*, 1994; *Bennett and Best*, 1995]. The main characteristics of the flow are (1) convergent, accelerated flow over the dune stoss, (2) flow separation at the dune crest, (3) flow reattachment at ~3.5-4.5 H [*Engel*, 1981], (4) a turbulent wake and shear layer originating at the crest, extending and expanding downstream, and (5) an outer, overlying wake region. Each region has diagnostic turbulence signatures that are important in sediment transport processes [*Nelson et al.*, 1993; *McLean et al.*, 1994; *Bennett and Best*, 1995]. Of particular interest here is the shear layer or wake region and its turbulence characteristics. This wake region resembles flow behind a cylinder [*McLean*, 1990], and three-dimensional rollers, kolks, and internal boils occur along the shear layer, dominating the macroturbulent flow structure.

Contour maps for all flow and turbulence parameters were constructed [*Venditti*, 1997], but only select results are presented here. Figure 4 shows profiles of time-averaged streamwise U, cross-stream V, and vertical W flow velocities defined as

$$U = \frac{1}{n}\sum_{i=1}^{n} u_i, \quad V = \frac{1}{n}\sum_{i=1}^{n} v_i, \quad W = \frac{1}{n}\sum_{i=1}^{n} w_i, \tag{1}$$

where u_i, v_i, and w_i are individual velocities and n is the total number of measurements. These profiles show the diagnostic characteristics as described above, including a well-developed shear layer. Rms velocities for the streamwise u, cross-stream v, and vertical w components, defined as

$$\text{rms}\, u = \left[\frac{1}{n}\sum_{i=1}^{n}(u_i - U)^2\right]^{0.5},$$

$$\text{rms}\, v = \left[\frac{1}{n}\sum_{i=1}^{n}(v_i - V)^2\right]^{0.5}, \tag{2}$$

$$\text{rms}\, w = \left[\frac{1}{n}\sum_{i=1}^{n}(w_i - W)^2\right]^{0.5},$$

are greatest near the separation cell, along the shear layer, and in near-bed regions (Figure 4), consistent with observations from previous studies [*Nelson et al.*, 1993; *McLean et al.*, 1994; *Bennett and Best*, 1995].

Profiles of velocity and their rms values compare favorably with those observed in the fixed bed experiments of *Bennett and Best* [1995]. Although the profiles are normalized by d and u_{*R}, these data are not identical, suggesting that quantitative similarity is restricted to small variations in dune shape, H/d, H/λ, and Fr.

3.2. Turbulent Flow Field

The spatial characteristics of turbulence over dunes can be defined by examining simple but informative turbulence and veloc-

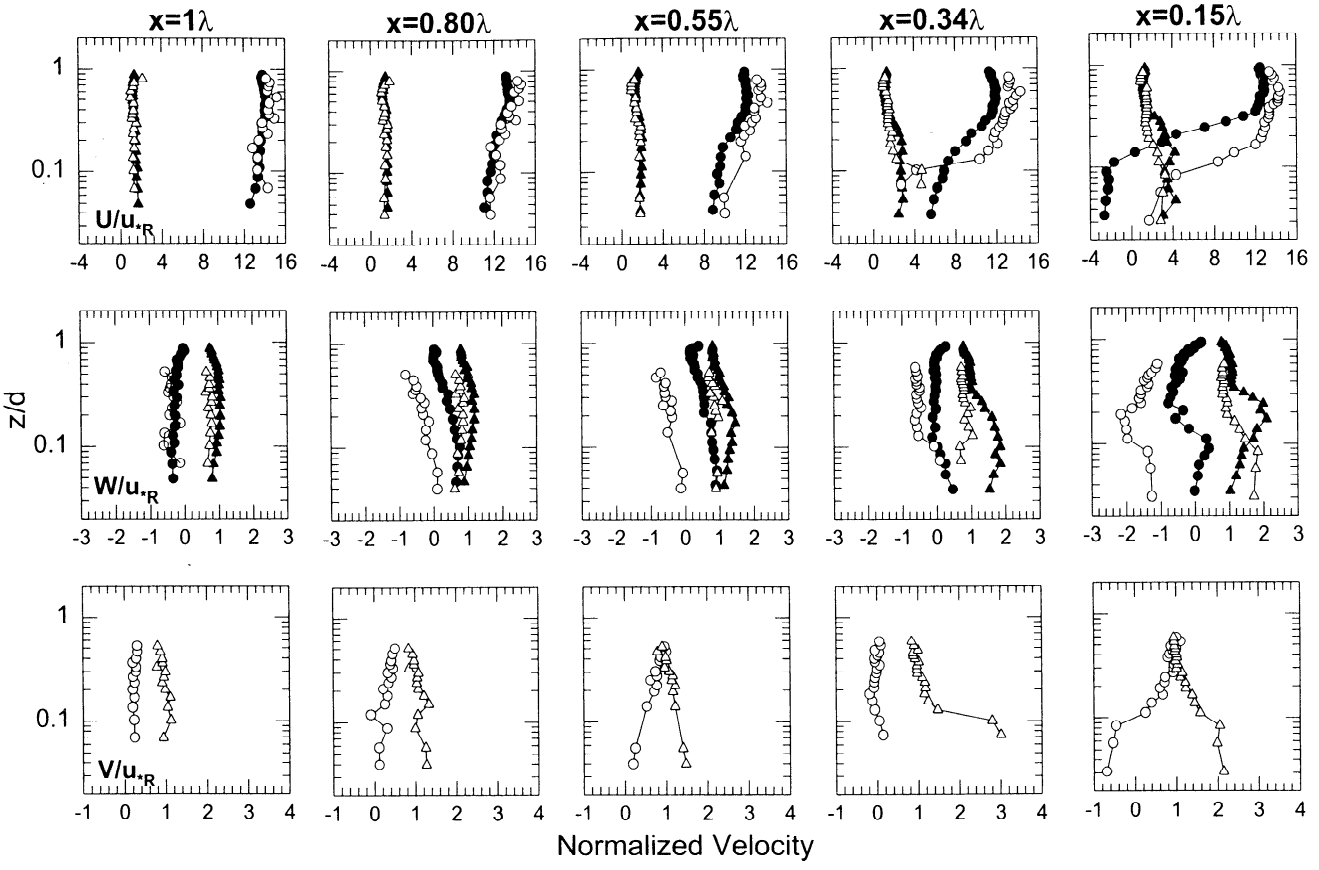

Figure 4. Select vertical profiles of streamwise (U) and vertical (W) flow velocity and their rms values (open symbols) normalized by u_{*R} and compared to profiles measured by *Bennett and Best* [1995] (solid symbols). Circles are mean values, and triangles are rms values. Also shown are the mean and rms values for the normalized cross-stream (V) velocity component. Positions are given relative to the dune length λ.

ity relations. Contour maps of select turbulence parameters are shown in Figure 5.

The spatial distribution of the Reynolds stress τ_{uw}, defined as

$$\tau_{uw} = -\rho\overline{u'w'}, \tag{3}$$

where $u' = u_i - U$, $w' = w_i - W$, and the overbar indicates a time average, delineates the wake region downstream of flow separation. Maximum values of τ_{uw}, as much as $3\tau_0$, occur within the separation cell, along the shear layer, and at flow reattachment (Figure 5a). Maxima of the other Reynolds stresses, τ_{uv} and τ_{vw}, also occurred within the separation cell and along the shear layer [*Venditti*, 1997], but both stresses tended toward zero in the rest of the flow field.

The distribution of τ_{uw} was used to calculate a spatially averaged bed shear stress τ_R. This was accomplished by averaging τ_{uw} along constant heights above the trough over one dune length and constructing a single Reynolds stress profile of the spatially averaged values [see *McLean et al.*, 1994; *Bennett and Best*, 1995]. A linear regression through τ_{uw} projected to the mean bed height resulted in $\tau_R = 1.69$ Pa, $u_{*R} = 0.041$ m s^{-1}, $\tau_R = 0.73\tau_0$, $u_{*R} = 0.85u_*$, and $ff_R = 0.064$ (Table 1).

A measure of structural coherence of the turbulence is the boundary layer correlation coefficient R_{uw}, defined as

$$R_{uw} = \frac{-\overline{u'w'}}{\text{rms}\,u \cdot \text{rms}\,w}. \tag{4}$$

R_{uw} can also be considered as a locally normalized Reynolds stress or simply a correlation between the streamwise and vertical velocity signals. Hence its distribution over the dune is closely correlated to the distribution of τ_{uw}. In clear water, flat bed flows, R_{uw} varies from 0.5 in near-bed regions and from 0.3-0 at 0.7-1.0d [*Nezu and Nakagawa*, 1993]. At the reattachment point and within the internal boundary layer, $R_{uw} \approx 0.2$-0.35, whereas in the outer flow region, $R_{uw} \approx 0.3$-0.5 (Figure 5b). In each of these regions, values of R_{uw} are similar to flat bed flows. Low values of R_{uw} within the internal boundary layer downstream of flow reattachment may be due to turbulent eddies intermittently impacting the bed [see *Nelson et al.*, 1993; *Müller and Gyr*, 1986]. In the wake region, $R_{uw} \approx 0.5$-0.6, and within flow separation, $R_{uw} \approx 0.6$-0.7. In these two regions, turbulence is strongly associated with τ_{uw} and the direct result of shear layer development. The separation cell and shear layer are the most turbulent areas over dunes, and structural coherence as defined by (4) is the greatest. Correlation coefficients using the other Reynolds stresses were close to zero and displayed no spatial dependency [*Venditti*, 1997].

The turbulent energy extracted from the mean flow by the motion of turbulent eddies [*Tennekes and Lumley*, 1972] is the turbulent kinetic energy (TKE), defined as

$$\text{TKE} = \frac{1}{2}\rho\left(\overline{u'^2} + \overline{v'^2} + \overline{w'^2}\right), \tag{5}$$

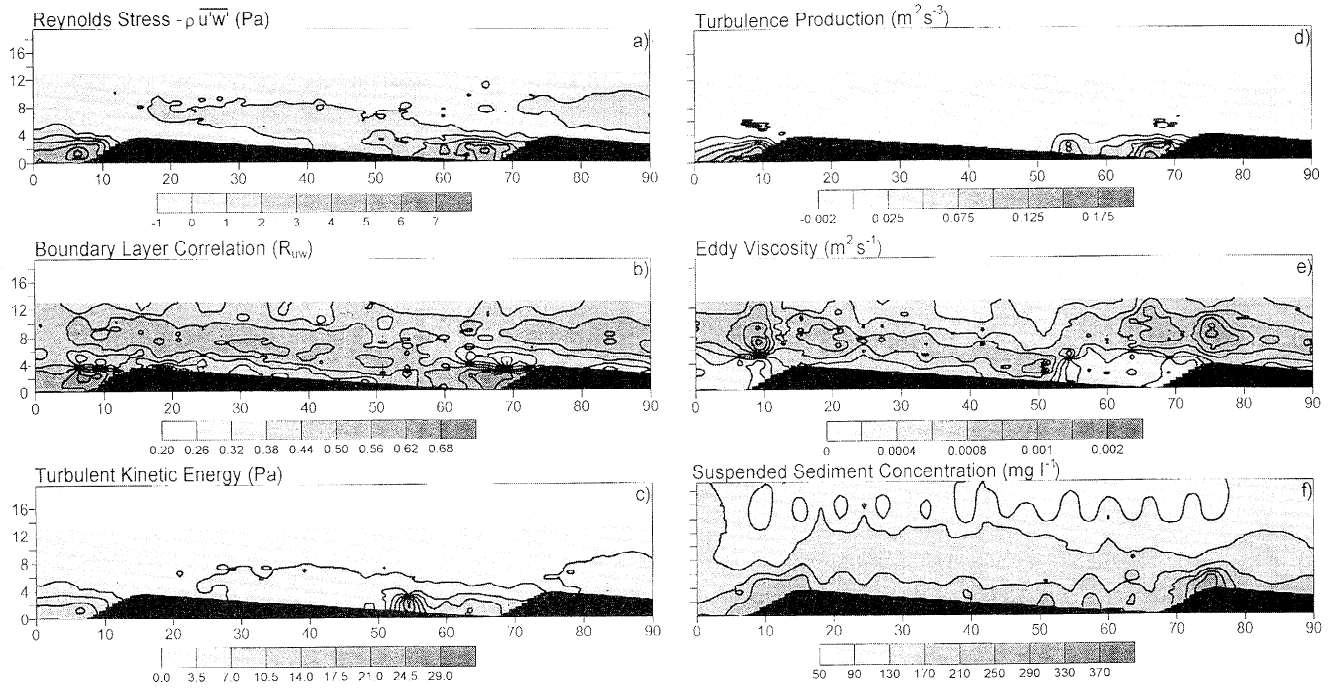

Figure 5. Contour maps of time-averaged turbulence quantities: (a) Reynolds stress τ_{uw}, (b) boundary layer correlation R_{uw}, (c) TKE, (d) turbulence production by vertical shear P, (e) eddy viscosity ε (diffusivity), and (f) suspended sediment concentration. Flow is from right to left, and horizontal and vertical axes are in centimeters.

and its production involves interactions of the Reynolds stresses with the mean velocity gradients (see below). Maximum values of TKE occur at reattachment, and large values occur within the separation cell (Figure 5c): at $5H$ and TKE $\approx 17\tau_R$. This TKE distribution highlights the importance of reattachment in the generation of highly turbulent eddies [*Iseya and Ikeda*, 1986; *Kostaschuk and Church*, 1993; *Nezu and Nakagawa*, 1993].

The magnitude of turbulence production by vertical shear P is defined as

$$P = -\overline{u'w'}\frac{\partial U}{\partial z}. \tag{6}$$

Because velocity gradients are nonlinear, high-order polynomials were fitted to determine $\partial U/\partial z$. Figure 5d shows that maximum turbulence production occurs within the flow separation cell and at flow reattachment.

Eddy viscosity ε, as defined in the mixing length concept, is the strength or magnitude of the turbulent eddies within the flow and is defined as

$$\varepsilon = \frac{-\overline{u'w'}}{\partial U/\partial z}. \tag{7}$$

The distribution of eddy viscosity should bear a strong relationship to P because $\varepsilon = P/(\partial U/\partial z)^2$. However, P varies over 3 orders of magnitude, while ε varies by a factor of 10, limiting any substantial comparison between their distributions in Figure 5. In flat bed flows the distribution of eddy viscosity is generally parabolic, reaching a maximum near $0.5d$ [*Bennett et al.*, 1998]. This parabolic distribution is the result of a linear decrease in τ_{uw} with z and a linear increase in U with ln z. As already shown, neither the distribution of τ_{uw} or of U is similar to flat bed flows. Thus eddy viscosity is strongly dependent upon bed form position and can vary by as much as an order of magnitude (Figure 5e). Over the dune crest the distribution of ε resembles a flat bed flow. In the flow separation cell, in the outer flow region, and near the bed, ε tends toward a minimum. The core of high ε values over the dune crest extends out over the separation cell, shifting downward toward the bed past reattachment as the internal boundary layer initiates and grows. Farther downstream, this core extends up and outward toward the next crest [see also *Nelson et al.*, 1993].

The parameters described above show that the separation cell and its associated flow structures dominate the turbulence characteristics over dunes. Large values of τ_{uw}, R_{uw}, and TKE characterize the separation cell and the shear layer. In these regions, $\tau_{uw} \approx 3\tau_0$ and $\tau_{uw} \approx 4\tau_R$. Large values of TKE and P clearly indicate the location of the reattachment point. The other Reynolds stresses, τ_{uv} and τ_{vw}, have little influence on fluid momentum transfer and macroturbulence generation. The structural coherence of the flow related to vertical shear is much higher within and near flow separation than in flat bed flows. Eddy viscosity can vary by an order of magnitude, and its distribution also shows this spatial dependence on bed form position.

3.3. Suspended Sediment Concentrations

Suspended sediment concentration varies both vertically within the flow and spatially along the dune (Figure 5f). Concentration reaches a maximum over the dune crest as bed load sediment moving along the stoss is suspended at flow separation and as sediment trapped within the separation cell is recirculated. In fact, the launch of sediment off the dune brink appears to account for nearly all the suspension (Figure 5f). The sediment concentration is high at flow reattachment where there is a double

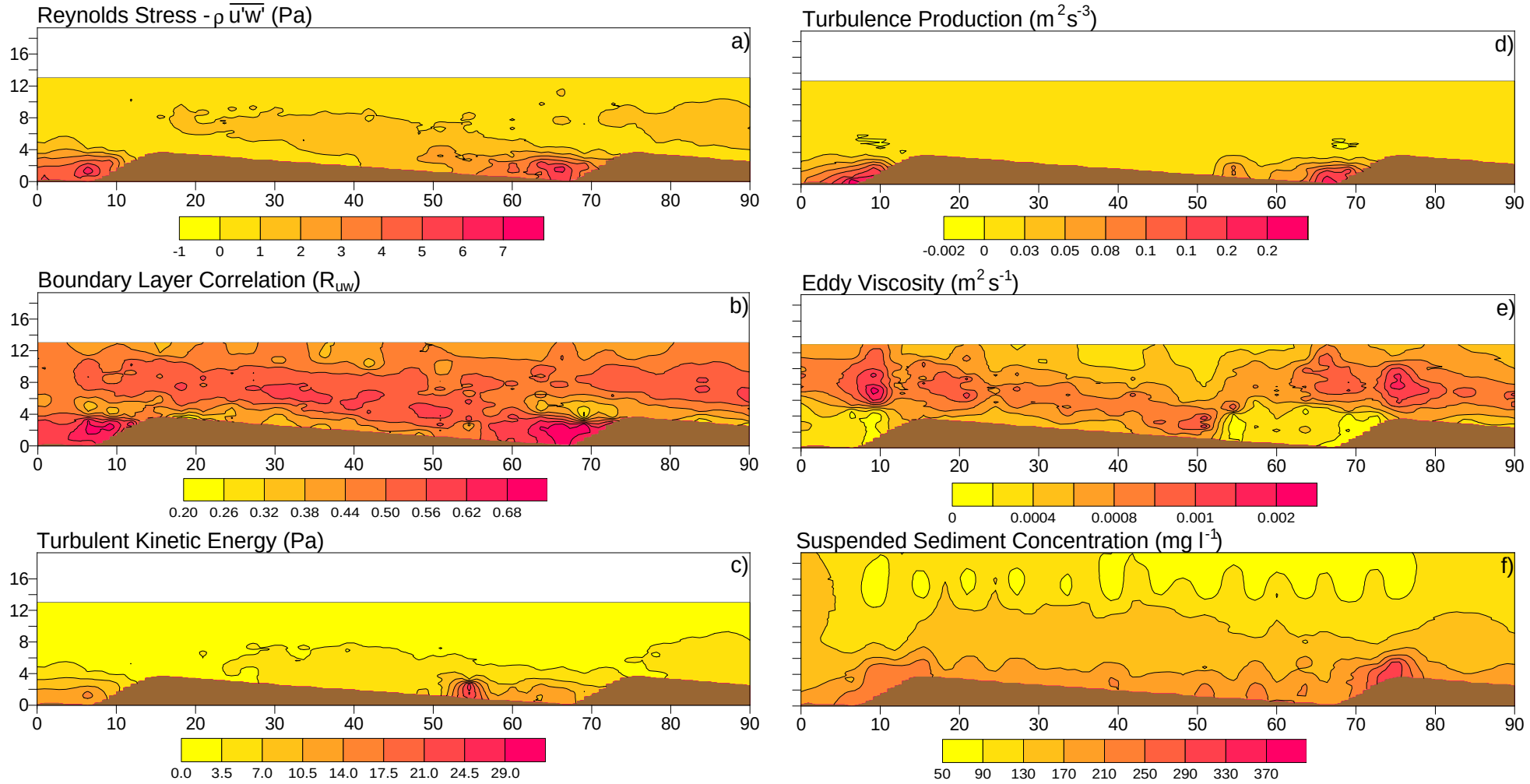
Reynolds Stress - ρ u'w' (Pa)
a)
16
12
8
4
0
0 10 20 30 40 50 60 70 80 90
-1 0 1 2 3 4 5 6 7
Turbulence Production (m2s-3)
d)
0 10 20 30 40 50 60 70 80 90
-0.002 0 0.03 0.05 0.08 0.1 0.1 0.2 0.2
Boundary Layer Correlation (Ruw)
b)
16
12
8
4
0
0 10 20 30 40 50 60 70 80 90
0.20 0.26 0.32 0.38 0.44 0.50 0.56 0.62 0.68
Eddy Viscosity (m2 s-1)
e)
0 10 20 30 40 50 60 70 80 90
0 0.0004 0.0008 0.001 0.002
Turbulent Kinetic Energy (Pa)
c)
16
12
8
4
0
0 10 20 30 40 50 60 70 80 90
0.0 3.5 7.0 10.5 14.0 17.5 21.0 24.5 29.0
Suspended Sediment Concentration (mg l-1)
f)
0 10 20 30 40 50 60 70 80 90
50 90 130 170 210 250 290 330 370

peak upstream and downstream of the peak in TKE (Figures 5c and 5f). Distribution of concentration also appears to be affected by the turbulent characteristics of the shear layer. As large values of τ_{uw} and ε extend outward into the flow downstream of reattachment, suspended sediment is advected along with these regions of high turbulence (see the 130 mg L^{-1} contour line, Figure 5f).

Shown in Figure 6 are profiles of suspended sediment flux $q_{s(z)}$ defined as

$$q_{s(z)} = C_{(z)} \cdot U_{(z)}, \tag{8}$$

where (z) represents at-a-point time averages and all necessary corrections for units are made. The largest sediment flux and the greatest vertical gradient in transport rate occur at the dune crest. Sediment flux decreases significantly in the dune trough (separation cell) because of low-flow velocities. The outer flow region shows very little vertical variation in suspended sediment flux. Spatially averaged suspended sediment transport rate is 0.065 kg m^{-1} s^{-1}.

4. Spectral Analysis

4.1. Velocity time series

Univariate spectral analysis was performed on velocity time series, the locations of which are identified in Figure 2. Since these locations have an approximately equal spacing in the streamwise direction, velocity spectra are plotted as eight sparse profiles in Figure 7. Each 82 s time series, corresponding to 2048 measurements, was detrended, and spectral estimates for each velocity component were calculated at 0.05 Hz intervals from 0 to 12.5 Hz using a bandwidth B_w of 0.8908 Hz in the spectral algorithm. By default, spectral results are biased toward the low-frequency range. Velocity spectra are plotted in variance-preserving form where spectral energy density $P(f)$ (cm^2 s^{-2} Hz^{-1}) is multiplied by frequency f [see *Soulsby*, 1977; *Panofsky and Dutton*, 1984; *Kaimal and Finnegan*, 1994]. The area under the spectrum of $f \cdot P(f)$ against $\log f$ represents the total variance, and peaks in the broad spectrum correspond to the frequency of an energetic mean or dominant eddy size passing the sensor [*Boppe and Neu*, 1995]. Confidence intervals for each spectrum were calculated using the χ^2 method where upper and lower confidence intervals are given by

$$\frac{B_w f \cdot P(f)}{\chi^2_{0.95}}, \quad \frac{B_w f \cdot P(f)}{\chi^2_{0.05}}, \tag{9}$$

respectively [*Jenkins and Watts*, 1968]. For each velocity spectrum the upper confidence interval is $1.2795\, f \cdot P(f)$ and the lower confidence interval is $0.8031\, f \cdot P(f)$ at the 95% confidence limit. Since the focus of the present study is to evaluate the distribution of energy in the frequency domain, these confidence intervals are not included in the plots of spectral energy.

Spectra for the velocity time series all generally peak from 1 to 4 Hz. The streamwise energy spectra generally peak at lower frequencies (~1-2 Hz; e.g., 6-45) than the vertical and cross-stream energy spectra (~2-4 Hz; e.g., 6-51, Figure 7). Differences between the peak frequencies in the streamwise spectra and other velocity components may be due to eddy shape: eddies may be elliptical as they advect and diffuse away from the shear layer presumably because streamwise eddy lengths are stretched and elongated by the mean flow. In the near-bed and wake regions, spectral energies are generally larger than in the rest of the flow field and have well-defined recurrence periods (e.g., 3-60, 3-51 6-36, 6-45, 9-51, and 9-45). Outside these regions, energies are smeared across a large frequency range and are generally smaller; that is eddies are not passing the sensors with a well-defined period but rather a range of sizes, trajectories, and magnitudes (e.g., 12-36, 12-69, and 12-75). Near the bed, there is a clear decline in the peak spectral energy from the region of flow reattachment.

The spatial distribution of the velocity spectra can be interpreted as characteristic of a perturbed shear layer having the following characteristics: (1) a "dead zone" or linear stability regime extending downstream of the dune crest that grows into a wave structure and (2) a nonlinear instability regime where Kelvin-Helmholtz waves develop and break along the shear layer that

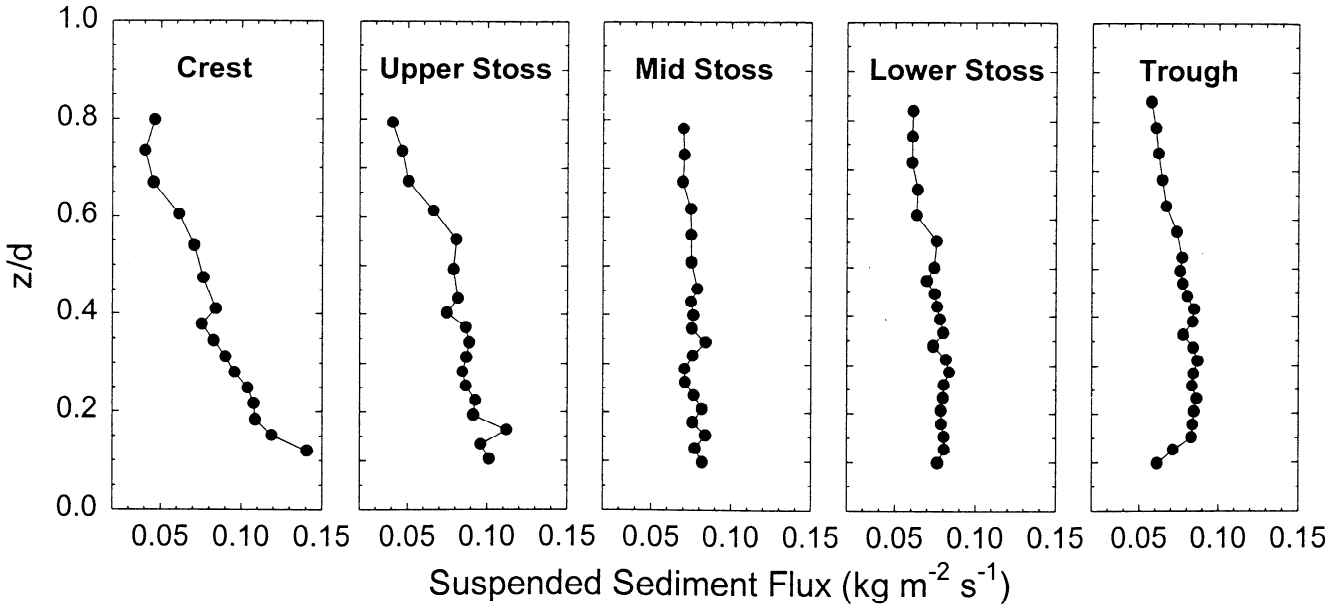

Figure 6. Selected vertical profiles of suspended sediment flux as a function of dune position.

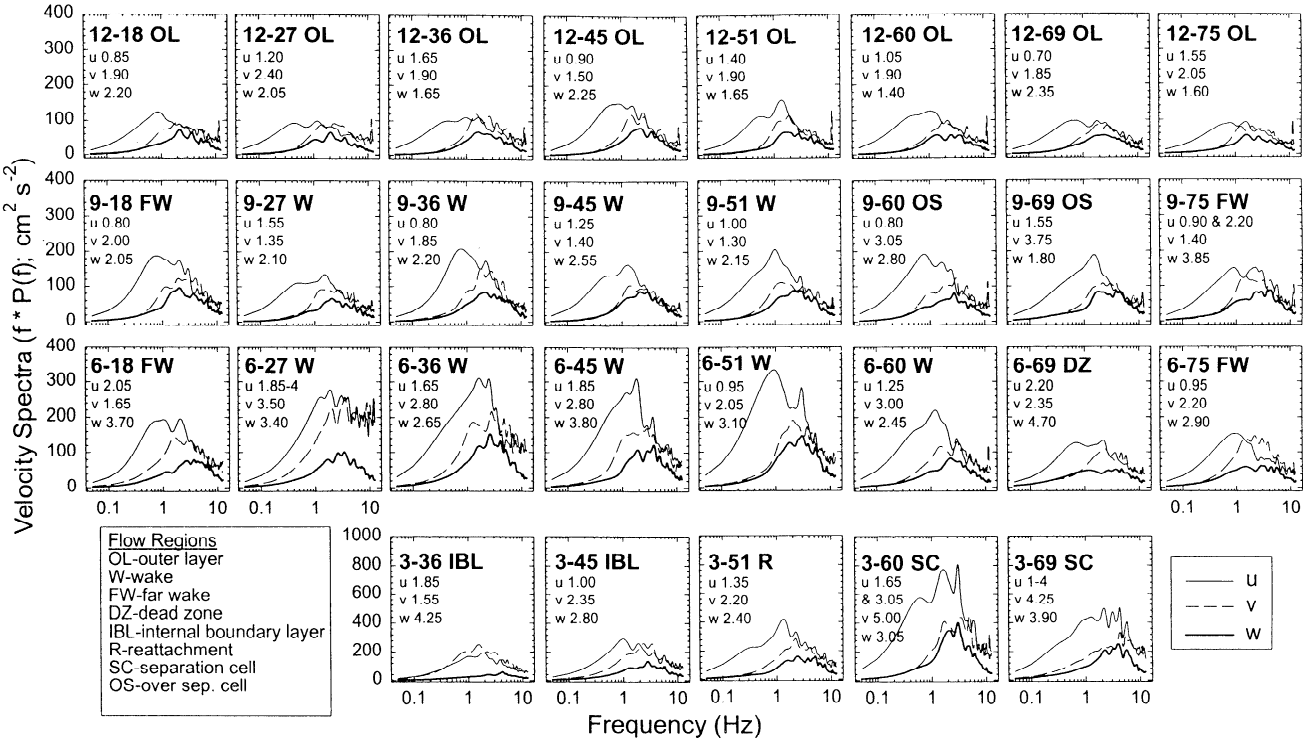

Figure 7. Spectral analysis of selected velocity time series (where 12-18 refers to a height of 12 cm above the trough and 18 cm upstream of the downstream end of the working section; see Figure 2a for locations). The peak frequencies for each velocity component within each specific flow region are shown in the upper left corner of each panel. Thin solid lines are the streamwise spectra, dashed lines are the cross-stream spectra, and thick solid lines are the vertical velocity spectra.

advect and diffuse vertically and downstream [see *Ho and Huerre*, 1984]. This pattern is exemplified in energy spectra along the shear layer and wake regions. Immediately downstream of the dune crest (location 6-69, Figure 7), little evidence exists that eddies pass the sensor with a single recurrence period because the spectra are flat over a wide range of frequencies (0.5-2 Hz). Farther downstream of the crest, spectra reveal this wave structure signature: sharper and well-defined peaks corresponding to larger variances than in the dead zone. This pattern suggests that eddies are Kelvin-Helmholtz instabilities along the shear layer as discussed in previous experimental [e.g., *Müller and Gyr*, 1982, 1986; *Bennett and Best*, 1995] and field studies [e.g., *Rood and Hickin*, 1989; *Kostaschuk and Church*, 1993].

Moving downstream and vertically from the perturbed shear layer, the magnitude of energy represented by the peak frequencies decreases, but the dominant frequency remains the same (Figure 7). Eddies produced along the shear layer diffuse and advect turbulent energy into the rest of the flow field, thus determining the characteristics of the velocity spectra. Above the shear layer, eddies mix and amalgamate with the mean flow structure, but relict frequencies (i.e., relict motions) still persist (Figure 7). Although turbulent energy may be derived from boundary layer and shear layer interactions, the dominant spectral signal originates along the shear layer, propagating downstream and vertically from this source. This spectral signature is presumably more distinct with maximum height bed forms than with bed waves of low relief.

The frequency f_s of eddies and shedding vortices in turbulent flows can be defined using a Strouhal number [*Levi*, 1983]

$$f_s = \frac{f l}{U}, \tag{10}$$

where l is a relevant length scale. For turbulent flow over dunes, l can be the bed form height H, the mean flow depth d, or the inner boundary layer depth. In the lee of the bed form, mean f_s for the u component is 0.52 using $l = d$ and 0.12 using $l = H$. These Strouhal numbers can be compared to other investigations characterizing eddy shedding from bed forms based on spectral and flow visualization techniques. For laboratory studies, f_s ranges from 0.33 to 0.50 using $l = d$ and 0.10 to 0.25 using $l = H$ [*Nezu et al.*, 1980; *Itakura and Kishi*, 1980; *Ikeda and Asaeda*, 1983; *Müller and Gyr*, 1986]. For field studies, f_s ranges from 0.30 to 0.38 using $l = d$ and 0.10 to 0.12 using $l = H$ [*Kostaschuk and Church*, 1993; *Venditti*, 1997]. The consistency of values is quite remarkable, demonstrating further that macroturbulence associated with a perturbed shear layer has diagnostic spectral characteristics. More detailed information on the variation of f_s over dune bed forms is given by *J.G. Venditti and B.O. Bauer* (manuscript in preparation, 2000).

4.2. Sediment Concentration Time Series

Time series of sediment concentration collected at the same time and location as the velocity time series were also selected for spectral analysis. Each OBS time series was detrended, and spectral estimates were calculated at 0.05 Hz intervals from 0 to 5 Hz using a bandwidth of 0.4711 Hz. A total of 102.4 s of concentration measurements was used corresponding to 1024 data points in each time series. For each concentration spectrum the

upper confidence interval is $1.4166\, f \cdot P(f)$ and the lower confidence interval is $0.7439\ f \cdot P(f)$ at the 95% confidence limit.

Energy spectra for the concentration data are shown in Figure 8. Because the magnitude of variance was unchanged by the corrections applied to the sediment concentration records, all spectra were normalized by the variance of each time series, producing spectra with a normalized energy ranging from 0 to 3. The normalization process applied negates any interpretation of the relative energy contained at a specific frequency (i.e., the area under the spectral curve), but the frequency information remains the same. Spectral energy peaks around 0.5 to 2 Hz, with the strongest peaks generally occurring at 1 Hz (e.g., 9-75, 9-60, and 3-36; Figure 8). These energy peaks appear to be coincident with the spectral peaks in the streamwise velocity component (Figure 7). Given the strongly peaked shapes of the concentration spectra, it appears that the suspended sediment is a very sharp delimiter of the most effective eddy scale. Values of f_s are 0.47 using $l = d$ and 0.11 using $l = H$, in agreement with nondimensional frequencies for the u component of velocity presented above.

5. Cospectral Analysis

Cospectral analysis, which included calculation of the cross spectrum and the squared coherency spectrum, was applied to the time series to examine further the link between sediment suspension and the production, advection, and diffusion of turbulence. Cross spectra show whether frequency components in one time series are associated with large or small fluctuations at the same frequency in the other time series. The squared coherency spectrum is a correlation coefficient defined at each frequency [*Jenkins and Watts*, 1968]. Cospectral analysis requires two time series to be sampled at the same frequency. Therefore the 25 Hz velocity time series were low-pass filtered to 10 Hz, interpolated to 100 Hz, and then resampled at 10 Hz. Comparison of the time series used in the cospectral analyses with the spectral analyses described above showed no difference in results. Each time series was detrended, and cospectral estimates were calculated at 0.05 Hz intervals from 0 to 5 Hz using a bandwidth of 0.4711 Hz in the cospectral algorithm. A total of 102.4 s of the velocity and concentration measurements were used corresponding to 1024 data points in each time series.

Cospectral analysis was performed at several locations within the flow field, but only one example is described here at a point near the bed and in the wake (6-45; see Figure 2 for location). Spectra at this location show a defined peak in the u component at 1.85 Hz and peaks in the w component at 1.90 and 3.80 Hz (Figure 7). The cross spectrum of u and w shows two strong peaks: at 1-2 (largest negative covariance at 1.70 Hz) and 3-5 Hz (Figure 9a). The squared coherency spectrum shows good correlation on the rising limb of the spectrum and again at ~1.65 Hz (Figure 9b). The secondary peak in the u against w cross spectrum is not recognized in the squared coherency spectrum, suggesting it is relatively unimportant when compared to the primary peak.

The concentration spectrum at this measurement location displays a strong peak at 1.65 Hz in agreement with the u against w cross spectrum (Figure 9c). Cross spectra of u against c, v against c, and w against c all appear to display some association between velocity components and concentration (Figure 9d). However, the squared coherency spectra fail to reveal any peak in the velocity spectra that can be correlated with the peak in the concentration spectrum (Figure 9e). Although it would appear qualita-

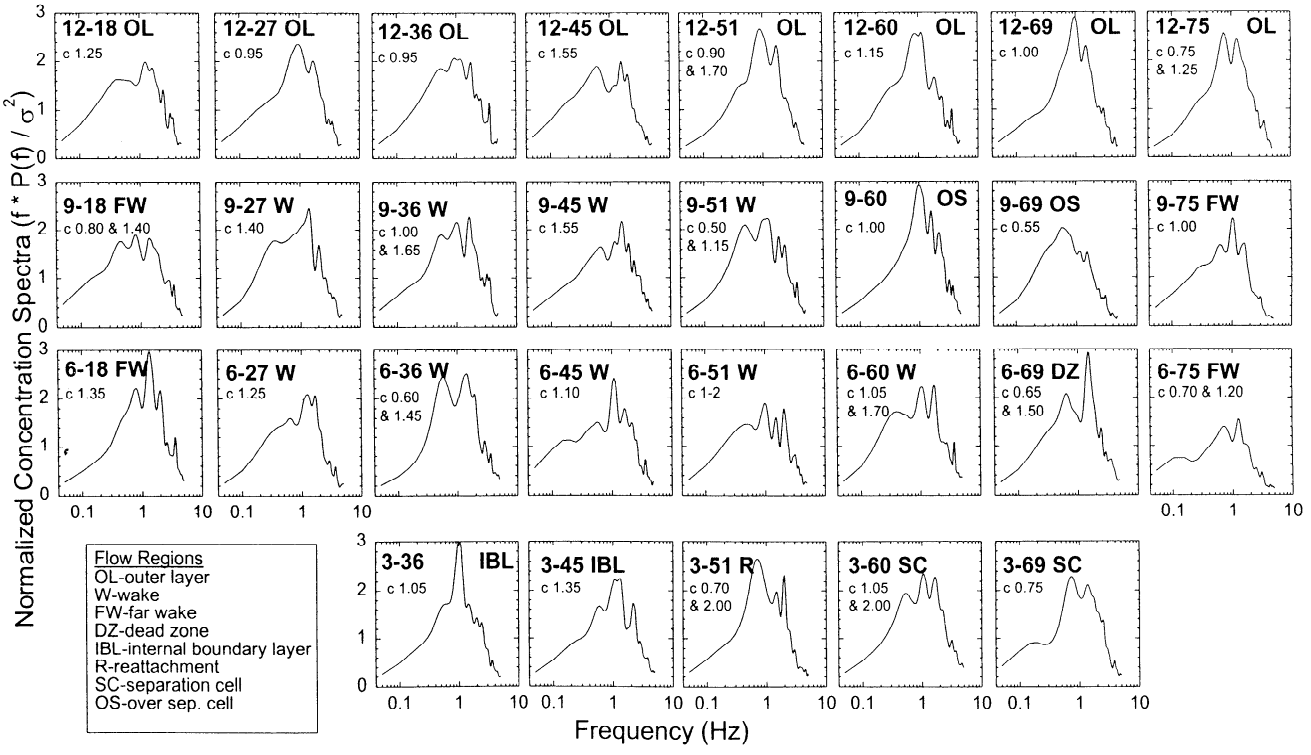

Figure 8. Spectral analysis of selected concentration time series normalized as described in text (where σ^2 is total variance; see Figure 2b for locations). Peak frequencies for concentration spectra are shown in the upper left corner of each panel.

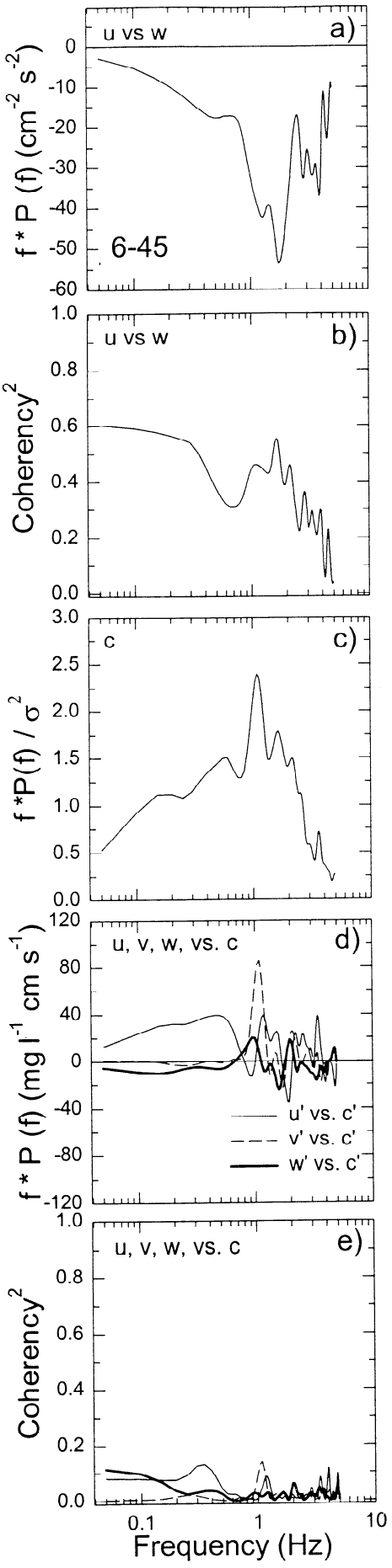

tively that some correlation between velocity and concentration is present, the cospectral results demonstrate that no such correlation exists. These cospectral results were observed systematically in all cases.

6. Integral Time and Length Scales

Autocorrelations for the velocity and concentration time series were derived to determine integral timescale and length scale. An integral timescale is the time an eddy requires to pass a given point in the flow, and an integral length scale is the characteristic eddy dimension. Corrections applied to the OBS time series for variable turbidity had no effect on the derived autocorrelation functions.

The Eulerian integral timescale T_E is defined as

$$T_E = \int_0^k R(t)dt, \tag{11}$$

where $R(t)$ is the autocorrelation function, dt is the lag distance, and k is the time step at which $R(t)$ is no longer significantly different from zero [*Tennekes and Lumley*, 1972]. In general, $R(t)$ approached zero asymptotically. In those cases when $R(t)$ approached and then oscillated about a zero value, k was determined when $R(t) = 0.01$. With a *Taylor* [1935] approximation the Eulerian integral length scale L_E is defined as

$$L_E = T_E \cdot U, \tag{12}$$

where U is measured at a point.

Integral timescales for the velocity components did not vary significantly with bed form position [*Venditti*, 1997], thus spatially averaged profiles of T_E are shown in Figure 10a. Timescales for the streamwise $T_{E(U)}$, cross-stream $T_{E(V)}$, and vertical $T_{E(W)}$ velocities are about 0.20, 0.06, and 0.06 s, respectively; $T_{E(U)} > T_{E(V)}, T_{E(W)}$ and $T_{E(V)} \approx T_{E(W)}$. Values of T_E for all velocity components are ~25% of the peak frequencies described above. Moreover, the integral timescale results parallel the spectral results: (1) the u component has a lower peak frequency and larger T_E as compared to the v and w components, and (2) the peak frequencies and T_E values for v and w are the same. Integral timescales for sediment concentration $T_{E(C)}$ range from 0.24 s near the bed to 0.30 s at 0.12 m above the trough (Figure 10a), and these values resemble more closely the u component results, i.e., $T_{E(C)} \approx T_{E(U)}$.

Streamwise eddy length scales $L_{E(U)}$ range from 0.065 m near the bed to 0.135 m at 0.12 m above the trough (Figure 10b) and are grossly related to height above bed, i.e., $L_{E(U)} \approx z$. Cross-stream $L_{E(V)}$ and vertical $L_{E(W)}$ integral length scales are nearly invariant with distance from the trough, ranging from 0.020 to 0.030 m, and are grossly related to dune (step) height, i.e., $L_{E(V)} \approx L_{E(W)} \approx H$. The integral length scale for concentration $L_{E(C)}$ increases with flow depth, from ~0.085 m near the bed to 0.160 m at 0.12 m above the trough (Figure 10b), similar to the u component, i.e., $L_{E(C)} \approx L_{E(U)} \approx z$.

Figure 9. Cospectral results for a measurement location in the near-bed region (6-45; see Figure 2) displaying (a) streamwise u velocity against vertical w velocity and (b) squared coherency spectrum. Also shown are (c) the concentration spectrum and (d) u against suspended sediment concentration c (thin solid curve), cross-stream v velocity against c (dashed curve), and w against c (thick solid curve) with the (e) squared coherency spectra.

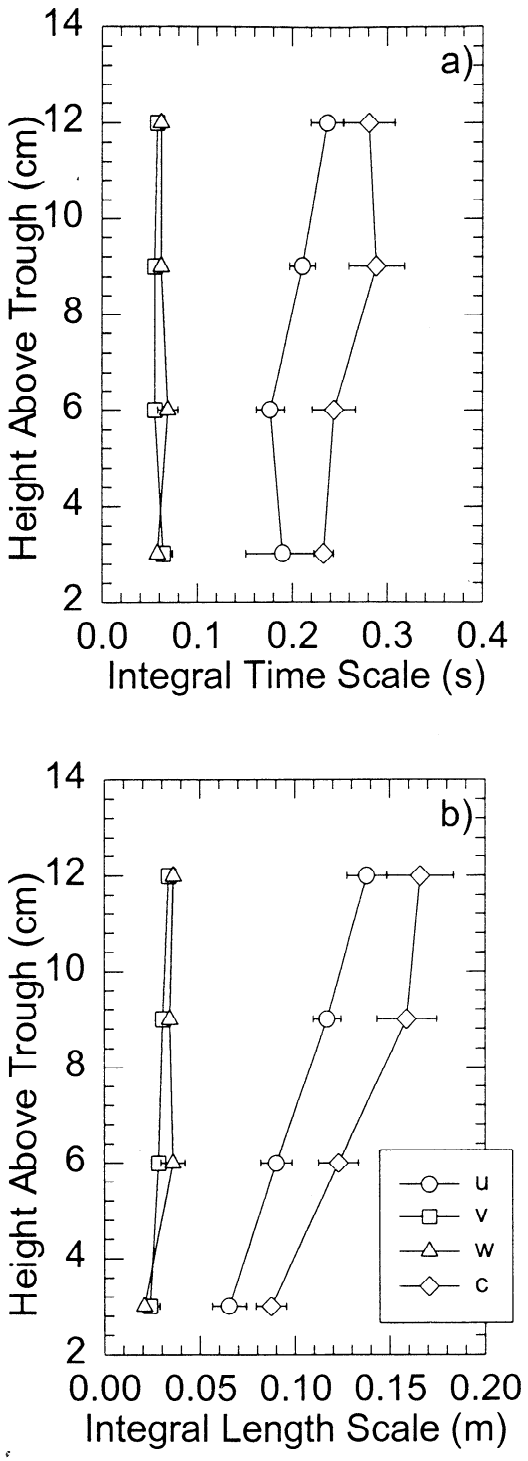

Figure 10. Vertical profiles of spatially averaged integral (a) timescale and (b) length scale. Refer to Figure 2 for locations. Error bars are standard error of the mean.

7. Conclusions

Laboratory measurements of turbulent fluctuations in velocity and suspended sediment concentration were obtained synchronously over fixed two-dimensional dunes using a sediment-starved flow. The observed turbulent flow field agrees well with observations in previous studies over both mobile and fixed dunes. High-magnitude Reynolds stresses (particularly τ_{uw}), TKE, and turbulence production due to vertical shear P characterize the separation cell, point of flow reattachment, and shear layer. Structural coherence of turbulence within and near the flow separation cell is much greater than that observed in flat bed flows. Eddy viscosity ε varies by an order of magnitude over the dune, and its distribution over the dune crest approaches that of a flat bed flow. Suspended sediment concentration is highest over the dune crest and at flow reattachment, and the advection of sediment into the outer flow is associated with the extension of the shear layer and its associated flow structures.

Spectral analysis of velocity time series reveals peak frequencies of 1-2 Hz for the streamwise component and 2-4 Hz for the cross-stream and vertical components. In near-bed and wake regions, spectra show larger and better defined peaks as compared to the rest of the flow field. The spatial distribution of energy spectra is interpreted as a perturbed shear layer where eddies form along a wave-like structure, likely a Kelvin-Helmholtz instability that dominates the spectral signature of the velocity time series. Suspended sediment concentration spectra reveal peak frequencies near 1 Hz, similar to the streamwise velocity, but these spectra show little variation over the dune bed form. Cospectral analysis demonstrates that no correlation exists between the velocity components and concentration despite similar univariate spectral signatures.

Integral timescales for the flow velocities range from 0.20 s for the streamwise component to 0.06 s for the cross-stream and vertical components, showing little variation along the dune. These timescales are ~25% of the observed peak frequencies. The integral timescale for concentration ranges from 0.24 to 0.30 s, similar to the streamwise component. The integral length scale for the streamwise component ranges from 0.065 m near the bed to 0.135 m at 0.12 m above the bed and is grossly related to flow depth. Cross-stream and vertical integral length scales range from 0.020 to 0.030 m and are grossly related to dune height. The integral length scale for concentration ranges from 0.085 m near the bed to 0.016 m at 0.12 m above the bed, similar to the streamwise velocity component.

Notation

B_w	bandwidth.
c, c_i, c', C	suspended sediment concentration, its instantaneous value, its fluctuation about the mean, and its mean value.
d	flow depth.
f	frequency.
ff, ff_R	Darcy-Weisbach friction factor calculated using τ_0 and τ_R.
f_n	Nyquist frequency.
f_s	nondimensional eddy shedding frequency
Fr	Froude number.
g	acceleration due to gravity.
H	dune height.
k	time step used for the autocorrelation functions.
l	length scale.
L_E, T_E	Eulerian integral length scale and timescale.
P	turbulence production.
$P(f)$	spectral energy.
q_s	suspended sediment flux.
R	hydraulic radius.
Re	Reynolds number.
R_{uw}	boundary layer correlation.

$R(t)$	autocorrelation function.
S	water surface slope.
t	time.
TKE	turbulent kinetic energy.
$u, u_i, U, \overline{U}$	streamwise velocity, its instantaneous value, its fluctuation about the mean, its mean value at a point, and its depth-averaged value.
u_*, u_{*R}	shear velocity calculated using τ_0 and τ_R.
v, v_i, V	cross-stream velocity, its instantaneous value, its fluctuation about the mean, and its mean value at a point.
w, w_i, W	vertical velocity, its instantaneous value, its fluctuation about the mean, and its mean value at a point.
z	height above the dune trough.
ε	eddy viscosity.
λ	dune wavelength.
ν	kinematic fluid viscosity.
ρ	fluid density.
σ^2	total variance of time series.
τ_0	boundary shear stress.
τ_R	spatially averaged Reynolds shear stress.
$\tau_{uw}, \tau_{uv}, \tau_{vw}$	Reynolds shear stresses.
ω_s	sediment fall velocity.

Acknowledgments. We gratefully acknowledge the technical support of J. Tuttle, M. Nelson, J. Cox, and J. Milan. P. Biron provided the algorithm to filter the ADV velocity signals. Financial support during data analysis was provided to J.V. through the Department of Geography at the University of Southern California and a University Graduate Fellowship at the University of British Columbia. B. Bauer provided valued comments and suggestions during data analysis. The manuscript has benefited by the constructive reviews of M. Church, R. Kuhnle, and M. Schmeeckle.

References

Ashworth, P.J., S.J. Bennett, J.L. Best, and S.J. McLelland, Eds., *Coherent Flow Structures in Open Channels*, 733 pp., John Wiley, New York, 1996.

Babakaiff, C.S., and E.J. Hickin, Coherent flow structures in Squamish River Estuary, British Columbia, Canada, in *Coherent Flow Structures in Open Channels*, edited by P.J. Ashworth et al., pp. 321-342, John Wiley, New York, 1996.

Bennett, S.J., and J.L. Best, Mean flow and turbulence structure over fixed, two-dimensional dunes: Implications for sediment transport and dune stability, *Sedimentology*, *42*, 491-513, 1995.

Bennett, S.J., J.S. Bridge, and J.L. Best, Fluid and sediment dynamics of upper stage plane beds, *J. Geophys. Res.*, *103*, 1239-1274, 1998.

Best, J., The fluid dynamics of small-scale alluvial bed forms, in *Advances in Fluvial Dynamics and Stratigraphy*, edited by P.A. Carling and M.R. Dawson, pp. 67-125, John Wiley, New York, 1996.

Best, J., S. Bennett, J. Bridge, and M. Leeder, Turbulence modulation and particle velocities over flat sand beds at low transport rates, *J. Hydraul. Eng.*, *123*, 1118-1129, 1997.

Biron, P., A.G. Roy, and J.L. Best, A scheme for resampling, filtering, and subsampling unevenly spaced laser Doppler anemometer data, *Math. Geol.*, *27*, 731-748, 1995.

Boppe, R.S., and W.L. Neu, Quasi-coherent structures in the marine atmospheric boundary layer, *J. Geophys. Res.*, *100*, 20,635-20,648, 1995.

Coleman, J.M., Brahmaputra River channel processes and sedimentation, *Sediment. Geol.*, *3*, 129-239, 1969.

Engel, P., Length of flow separation over dunes, *J. Hydraul. Div. Am. Soc. Civ. Eng.*, *107*, 1133-1143, 1981.

Flemming, B.W., Zur klassifikation subaquatistischer, stromungstrans versaler transportkorper, *Boch. Geol. Univ. Geotechnol. Arb.*, *29*, 44-47, 1988.

Guy, H.P., D. B. Simons, and E.V. Richardson, Summary of alluvial channel data from flume experiments, 1956-1961, *U.S. Geol. Surv. Prof. Pap.*, *462-I*, 96 pp., 1966.

Hay, A.E., and A.J. Bowen, Coherence scales of wave-induced suspended sand concentration fluctuations, *J. Geophys. Res.*, *99*, 12,749-12,765, 1994.

Hay, A.E., and J. Sheng, Vertical profiles of suspended sand concentration and size from multifrequency acoustic backscatter, *J. Geophys. Res.*, *97*, 15,661-15,677, 1992.

Ho, C., and P. Huerre, Perturbed free shear layers, *Annu. Rev. Fluid Mech.*, *16*, 365-424, 1984.

Ikeda, S., and T. Asaeda, Sediment suspension with rippled bed, *J. Hydraul. Eng.*, *109*, 409-423, 1983.

Iseya, F., An experimental study of dune development and its effect on sediment suspension, Environ. Res. Cent. Pap. 5, 56 pp., Univ of Tsukuba, Tsukuba, Japan, 1984.

Iseya, F., and H. Ikeda, Effect of dune development on sediment suspension under unsteady flow conditions, paper presented at 30th Japanese Conference on Hydraulics, Jpn. Soc. of Civ. Eng., 1986.

Itakura, T., and T. Kishi, Open channel flow with suspended sediments on sand waves, in *Proceedings of the Third International Symposium on Stochastic Hydraulics*, edited by H. Kikkawa and Y. Iwasa, pp. 589-598, Int. Assoc. of Hydraul. Res., Tokyo, Japan, 1980.

Jackson, R.G., Sedimentological and fluid-dynamic implications of the turbulent bursting phenomenon in geophysical flows, *J. Fluid Mech.*, *77*, 531-560, 1976.

Jenkins, G.M., and D.G. Watts, *Spectral Analysis and Its Applications*, 525 pp., Merrifield, Va., 1968.

Kaimal, J.C., and J.J. Finnegan, *Atmospheric Boundary Layer Flows: Their Structure and Measurement*, 289 pp., Oxford Univ. Press, New York, 1994.

Korchokha, Y.M., Investigation of the dune movement of sediments on the Polomet River, *Sov. Hydrol.*, *11*, 541-559, 1968.

Kostaschuk, R.A., and M.A. Church, Macroturbulence generated by dunes: Fraser River, Canada, *Sediment. Geol.*, *85*, 25-37, 1993.

Lane, S.N., P.M. Biron, K.F. Bradbrook, J.B. Butler, J.H. Chandler, M.D. Crowell, S.J. McLelland, K.S. Richards, and A.G. Roy, Three-dimensional measurement of river channel flow processes using acoustic Doppler velocimetry, *Earth Surf. Processes Landforms*, *23*, 1247-1267, 1998.

Lapointe, M.F., Burst-like sediment suspension events in a sand bed river, *Earth Surf. Processes Landforms*, *17*, 253-270, 1992.

Lapointe, M.F., Frequency spectra and intermittency of the turbulent suspension process in a sand-bed river, *Sedimentology*, *43*, 439-449, 1996.

Levi, E., A universal Strouhal law, *J. Hydraul. Eng.*, *109*, 718-727, 1983.

Lohrmann, A., R. Cabrera, and N.C. Kraus, Acoustic-Doppler velocimeter (ADV) for laboratory use, paper presented at Fundamentals and Advancements in Hydraulic Measurements and Experimentation, Am. Soc. of Civ. Eng., Buffalo, N.Y., 1994.

Matthes, G.H., Macroturbulence in natural stream flow, *EOS Trans. AGU*, *28*, 255-262, 1947.

McLean, S.R., The stability of ripples and dunes, *Earth Sci. Rev.*, *29*, 131-144, 1990.

McLean, S.R., J.M. Nelson, and S.R. Wolfe, Turbulence structure over two-dimensional bed forms: Implications for sediment transport, *J. Geophys. Res.*, *99*, 12,729-12,747, 1994.

McLean, S.R., J.M. Nelson, and R.L. Shreve, Flow-sediment interactions in separating flows over bed forms, in *Coherent Flow Structures in Open Channels*, edited by P.J. Ashworth et al., pp. 203-226, John Wiley, New York, 1996.

Müller, A., and A. Gyr, Visualization of the mixing layer behind dunes, in *Mechanics of Sediment Transport*, edited by B.M. Sumer and A. Müller, pp. 41-45, A.A. Balkema, Brookfield, Vt., 1982.

Müller, A., and A. Gyr, On the vortex formation in the mixing layer behind dunes, *J. Hydraul. Res.*, *24*, 359-375, 1986.

Nelson, J.M., S.R. McLean, and S.R. Wolfe, Mean flow and turbulence fields over two-dimensional bed forms, *Water Resour. Res.*, *29*, 3935-3953, 1993.

Nezu, I., and H. Nakagawa, *Turbulence in Open-Channel Flows*, Int. Assoc. Hydraul. Res. Monogr. Ser., 281 pp., A.A. Balkema, Brookfield, Vt., 1993.

Nezu, I., H. Nakagawa, A. Tominaga, and M. Yoshikawa, Visual study of large-scale vortical motions in open-channel flow, paper presented at Annual Conference of the Japanese Society of Civil Engineers, Kansai-Branch, 1980.

Nielsen, P., *Coastal Bottom Boundary Layers and Sediment Transport*, 324 pp., World Sci., River Edge, N.J., 1992.

Nielsen, P., Sediment suspension modelling in terms of combined convection diffusion, in *Sediment Transport Mechanisms in Coastal Envi-*

ronments and Rivers, EUROMECH 310, edited by M. Bélorgey, R.D. Rajaona, and J.F.A. Sleath, pp. 79-92, World Sci., River Edge, N.J., 1994.

Osborne, P.D., and B. Greenwood, Frequency dependent cross-shore suspended sediment transport, 1, A non-barred shoreface, *Mar. Geol.*, *106*, 1-24, 1991a.

Osborne, P.D., and B. Greenwood, Frequency dependent cross-shore suspended sediment transport, 2, A barred shoreface, *Mar. Geol.*, *106*, 25-54, 1991b.

Osborne, P.D., and B. Greenwood, Sediment suspension under waves and currents: Time scales and vertical structure, *Sedimentology*, *40*, 599-622, 1993.

Panofsky, H.A., and J.A. Dutton, *Atmospheric Turbulence: Models and Methods for Engineering Applications*, 390 pp., Wiley, New York, 1984.

Parker, G., Some speculations on the relation between channel morphology and channel-scale flow structures, in *Coherent Flow Structures in Open Channels*, edited by P.J. Ashworth et al., pp. 423-458, John Wiley, New York, 1996.

Rood, K.M., and E.J. Hickin, Suspended sediment concentration in relation to surface-flow structure in Squamish River estuary, southwestern British Columbia, *Can. J. Earth Sci.*, *26*, 2172-2176, 1989.

Soulsby, R.L., Similarity scaling of turbulence spectra in marine and atmospheric boundary layer, *J. Phys. Oceanogr.*, *10*, 934-937, 1977

Taylor, G.I., Statistical theory of turbulence: Parts 1-4, *Proc. R.. Soc. London, Ser. A*, *151*, 421-511, 1935.

Tennekes, H., and J.L. Lumley, *A First Course in Turbulence*, 300 pp., MIT Press, Cambridge, Mass., 1972.

Thorne, P.D., P.J. Hardcastle, and R.L. Soulsby, Analysis of acoustic measurements of suspended sediment, *J. Geophys. Res.*, *98*, 899-910, 1993.

Thorne, P.D., P.J. Hardcastle, and A. Hogg, Observations of near-bed suspended sediment turbulence structures using multifrequency acoustic backscattering, in *Coherent Flow Structures in Open Channels*, edited by P.J. Ashworth et al, pp. 281-304, John Wiley, New York, 1996.

van Rijn, L.C., *Principles of Sediment Transport in Rivers, Estuaries, and Coastal Seas*, Aqua, Amsterdam, 1994.

Venditti, J.G., *Spatial and Temporal Turbulence Structure over Sub-Aqueous Dunes: Field and Laboratory Experiments*, M.Sc. thesis, 131 pp., Univ. of South. Calif., Los Angeles, 1997.

Willis, J.C., An error function description of the vertical suspended sediment distribution, *Water Resour. Res.*, *5*, 1322-1329, 1969.

S. J. Bennett, U.S. National Sedimentation Laboratory, Department of Agriculture, Agricultural Research Service, P.O. Box 1157, Oxford, MS 38655. (bennett@sedlab.olemiss.edu)

J. G. Venditti, Department of Geography, University of British Columbia, 217-1984 West Mall, Vancouver, British Columbia, V6T 1Z2, Canada. (e-mail: venditti@geog.ubc.ca)

(Received January 25, 1999; revised December 23, 1999; accepted March 27, 2000.)